ORIGINAL ARTICLE

# A subcutaneous pancreatic islet transplantation platform using a clinically applicable, biodegradable Vicryl mesh scaffold - an experimental study

Hirotake Komatsu[1], Nelson Gonzalez[1], Mayra Salgado[1], Colin A. Cook[2], Junfeng Li[1], Jeffrey Rawson[1], Keiko Omori[1], Yu-Chong Tai[2], Fouad Kandeel[1] & Yoko Mullen[1]

1 Department of Translational Research & Cellular Therapeutics, Beckman Research Institute of City of Hope, Duarte, CA, USA
2 Department of Electrical Engineering, California Institute of Technology, Pasadena, CA, USA

**Correspondence**
Hirotake Komatsu MD, PhD, Department of Translational Research & Cellular Therapeutics, Beckman Research Institute of City of Hope, 1500 E. Duarte Rd., Duarte, CA 91010, USA.
Tel.: +1-626-359-8111 ext. 60971;
fax: +1-626-301-8136;
e-mail: hkomatsu@coh.org

## SUMMARY

Pancreatic islet transplantation into the liver is an effective treatment for type 1 diabetes but has some critical limitations. The subcutaneous site is a potential alternative transplant site, requiring minimally invasive procedures and allowing frequent graft monitoring; however, hypoxia is a major drawback. Our previous study without scaffolding demonstrated post-transplant graft aggregation in the subcutaneous site, which theoretically exacerbates lethal intra-graft hypoxia. In this study, we introduce a clinically applicable subcutaneous islet transplantation platform using a biodegradable Vicryl mesh scaffold to prevent aggregation in a diabetic rat model. Islets were sandwiched between layers of clinically proven Vicryl mesh within thrombin-fibrin gel. *In vitro*, the mesh prevented islet aggregation and intra-islet hypoxia, which significantly improved islet viability. *In vivo* rat syngeneic islet transplantations into a prevascularized subcutaneous pocket demonstrated that the mesh significantly enhanced engraftment, as measured by assays for graft survival and function. Histological examination at 6 weeks showed well-vascularized grafts sandwiched in a flat shape between the mesh layers. The biodegradable mesh was fully absorbed by three months, which alleviated chronic foreign body reaction and fibrosis, and supported long-term graft maintenance. This simple graft shape modification approach is an effective and clinically applicable strategy for improved subcutaneous islet transplantation.

*Transplant International* 2020; 33: 806–818

**Key words**
biodegradable mesh scaffold, hypoxia, oxygenation, pancreatic islet, subcutaneous cell transplantation, Vicryl mesh

Received: 7 December 2019; Revision requested: 27 December 2019; Accepted: 17 March 2020;
Published online: 14 April 2020

## Introduction

Cell transplantation is a promising treatment in which lost cellular function is complemented by transplanting new cells with the relevant specific function. Recent advancements in stem cell research have shed light on this treatment option for hematopoietic disorders (bone marrow transplantation) [1,2], peripheral nerve injury (Schwann-like cells) [3,4], and diabetes (beta cell transplantation) [5-7]. This concept is exemplified by




doi:10.1111/tri.13607

pancreatic islet transplantation as a treatment for type 1 diabetes (T1D), in which insulin-producing islets are isolated from deceased donors and infused into a recipient's liver through the portal vein [8]. Subsequently, T1D patients benefit from improved glycemic control, including reduced risks of secondary complications and lethal hypoglycemia due to excessive insulin injections [9,10].

Although the conventional strategy of transplanting islets into the liver is effective to a certain extent, conditions in the liver microenvironment and innate immune responses, including the instant blood-mediated inflammatory response (IBMIR), often lead to acute as well as gradual loss of transplanted islet grafts [11,12]. Thus, development of alternative islet transplantation sites, such as the subcutaneous (SC) site, is of great interest. The SC site provides extensive space for transplanted cells and allows minimally invasive transplantation procedures. The SC site also offers obvious advantages over other sites for stem cell-derived, insulin-producing cell transplantation, due to the feasibility of frequent graft monitoring, early detection of any potential malignancies, and graft retrievability when needed.

Despite these advantages, SC islet transplantation is not yet practical; limited vascularity and low oxygen ($O_2$) are major obstacles to efficient engraftment [13]. Modulation of vascularity prior to transplantation (i.e., prevascularization) has been recognized as an essential procedure for enhancing engraftment in rodent models by improving the replenishment of $O_2$ to the graft site [13-17]. However, islet engraftment in the SC site is still less efficient compared to that in the liver, even with prevascularization, unless the site is actively oxygenated [13].

To further improve the efficiency of islet transplantation in the SC site, supplementation with nutrients and oxygen and application of scaffolds have been introduced [18-22]. Scaffolds, including hydrogels, are often functionalized with proangiogenic factors and extracellular matrix (ECM) to enhance revascularization and sustain islet function [23-26]. Furthermore, enhancement of small molecule (e.g., $O_2$) diffusion, achieved by spreading individual islets to prevent aggregation, is also an important function of a scaffold. Because the distance across which $O_2$ diffuses in the tissue and islet graft is quite limited and because islet cells are susceptible to hypoxia, islet graft size matters [27,28]. We showed that whereas islets transplanted into the liver were dispersed into the peripheral branches of the portal vein (Fig. S1a,b), subcutaneously transplanted islets without scaffolding formed large aggregates (Fig. S1c,d); such pronounced aggregation could induce severe intragraft hypoxia. For clinical application of SC islet transplantation, which will require large numbers of cells and a correspondingly large graft bed, graft aggregation is likely to be a serious problem, resulting in hypoxia-induced graft death.

Another major issue with clinical use of scaffolds is the potential for chronic foreign body reaction to the material, which could result in inflammation-induced graft fibrosis and attrition [29,30]. Biodegradable materials are advantageous in alleviating such chronic foreign body reactions. Scaffolds are theoretically not required for supporting islets once a graft is well revascularized and nutrients and $O_2$ are efficiently and directly transported via the vascular network into the graft. Therefore, biodegradation of a scaffold could occur after completion of revascularization, which takes 10 days–1 month [31-35].

In this paper, we introduce a clinically applicable approach to SC islet transplantation using biodegradable mesh (Vicryl mesh, generally used in clinical hernia repair surgeries) in a rat SC transplantation model. We demonstrate an effective method of sandwiching islets to prevent aggregation and show that the $O_2$ microenvironment of the scaffolded islets is improved. We also demonstrate that use of a biodegradable scaffold is advantageous over long-term observation.

## Materials and methods

### Preparation of the mesh

VICRYL® Woven Mesh (Ethicon, Somerville, NJ, USA), a clinically proven, synthetic biodegradable material (polyglactin 910) [36,37], was modified for SC islet transplantation. The original mesh, which is tightly woven, was manually enlarged under a dissection microscope to a 200 μm-sized mesh.

### Isolation of rat pancreatic islets

Male Lewis (LEW) rats weighing 400–500 g were used as pancreas donors for islet isolation using our standard procedure [38]. In experiments requiring the measurement of bioluminescent intensity of islets post-transplantation (specified in *Observation of islet recipients*), luciferase (LUC) transgenic LEW rats were used as donors [39].

### Islet culture for Vicryl mesh experiments

Isolated islets were cultured either with or without Vicryl mesh. Solutions of thrombin and fibrinogen

(both from rat plasma; Sigma-Aldrich, St. Louis, MO, USA) were prepared as previously described [22,40] and mixed with islets for gelation. Three hundred rat islets were embedded in 6 μl of thrombin–fibrin gel. For control groups (without mesh), islets were mixed with thrombin–fibrin gel and placed on a polycarbonate cell insert (Millipore, Burlington, MA, USA). For mesh groups, islets were mixed with thrombin–fibrin gel, sandwiched between 5 × 5-mm Vicryl mesh layers, and placed on a cell insert. Islets were cultured in RPMI 1640 (Life Technologies, Grand Island, NY, USA) supplemented with 10% FBS and 5 mM glucose at 37 °C in a tissue culture incubator under 21% $O_2$ plus 5% $CO_2$ for 7 days (culture medium was replaced on day 3).

### Islet volume assessment

Islet functional volume was assessed *in vitro* using an ATP-based bioluminescent intensity assay, using LUC transgenic rat-derived isolated islets. Seven-day cultured islets with or without mesh were incubated in luciferin solution (PerkinElmer, Waltham, MA, USA; 150 μg/ml dissolved in the culture medium) for 10 min; then, ATP activity was measured (Lago X platform, Spectral Instruments Imaging, Tucson, AZ, USA). Experiments were repeated using islets from three different donors.

### *In vitro* viability assay

Islet viability was analyzed using fluorescein diacetate (FDA) and propidium iodide (PI) by a semi-automated method, as previously described [41]. Islets cultured for 7 days were retrieved for analysis; islets sandwiched by meshes were retrieved by removing the top mesh layer and gently flushing islets using culture medium. Size assessments of isolated islets were performed using data collected from viability assay images (cellSens, version 1.12; Olympus, Tokyo, Japan). Experiments were repeated using islets from three different donors.

### *In vitro* islet function assay

Glucose-stimulated insulin secretion (GSIS) assays were performed using a static incubation method [three phases in Krebs–Ringer buffer glucose solution: 2.8 mM (low-1), 28 mM (high), and 2.8 mM (low-2); 1 h/phase]. Data were normalized using total insulin content in islets [42]. Data from the first two phases were used to determine the stimulation index, as described previously [43]. Experiments were repeated using islets from five different islet isolations.

### Hypoxia-related gene expression analysis

Islets were obtained for RNA isolation 7 days after *in vitro* culture of both control and mesh groups, followed by real-time PCR, as described previously [13]. Relative quantities of each transcript (hypoxia-related genes) were normalized to an endogenous housekeeping gene (*ACTB*) and expressed as fold increase to controls. All primers for *HIF1A* (Rn01472831_m1), *VEGFA* (Rn01511602_m1), *GAPDH* (Rn01775763_g1), *SLC2A1* (Hs00892681_m1), and *ACTB* (Rn00667869_m1) were obtained from Thermo Fisher Scientific (Waltham, MA, USA).

### Computational simulation of $O_2$ distribution inside islets

Finite-element simulations of $O_2$ inside islets and aggregates were performed using COMSOL 5.3 (COMSOL, Los Angeles, CA, USA) [27]. Dissolved $O_2$ in rat SC tissues (45 mmHg) and $O_2$ consumption rate by islets were measured as major parameters determining the $O_2$ inside islets and aggregates for the simulation [13]. Given the negligible $O_2$ permeability of polyglactin compared to water, the $O_2$ permeability of the mesh layer was taken as that of water scaled by the projected, open cross-sectional area of the mesh (~50%). Other parameters for the simulation, including diffusivity and solubility of $O_2$ in islets and the Michaelis $O_2$ constant, were used as previously described [44-46].

### Islet transplantation

For islet recipients, syngeneic female LEW rats weighing 180–200 g (10–16 weeks old, analogous to young human patients) were rendered diabetic by a single intravenous injection of streptozotocin (STZ; 60 mg/kg; Sigma-Aldrich) as an insulin-dependent diabetes model. Because an adequate number of transplanted islets per body weight are required to achieve diabetes reversal in islet transplantations [13], rapid body weight gain during the transplant period may affect the outcome. To eliminate body weight increase bias, we used female LEW rats, in which body weight increase is approaching a plateau and is slower than that in male rats at this age [47]. Prior to transplantation, a prevascularized SC graft bed was prepared by implanting a lyophilized agarose-basic fibroblast growth factor (bFGF) disk into recipient rats, as described previously [13]. Islet grafts (600 islets or 750 islets) were prepared from male LEW donors in the same manner described above for *in vitro* islet

culture, but using 12 μl of thrombin–fibrin gel. For mesh groups, islets in thrombin–fibrin gel were sandwiched between 7 × 7-mm Vicryl mesh layers. Grafts were transplanted into prevascularized capsules in recipient rats. In a separate experiment, islet transplantations (600 islets) into the liver were performed via the portal vein (injection from the mesenteric vein), using the same rat model described above, to demonstrate islet distribution in the liver [38]. The use of animals and animal procedures performed in this study were approved by the City of Hope/Beckman Research Institute Institutional Animal Care and Use Committee.

### Observation of islet recipients

Islet recipients were monitored for 6 weeks after transplantation for short-term experiments and for 12 weeks after transplantation for long-term experiments. In short-term experiments, nonfasting blood glucose levels and body weight were measured biweekly. LUC-bioluminescent intensity-based *in vivo* graft viability (weeks 1 and 3) and intraperitoneal glucose tolerance test (IPGTT) and glucose-stimulated C-peptide measurements (week 5) were performed [13,48]. In long-term experiments, nonfasting blood glucose levels were measured biweekly. Rats were euthanized to remove islet grafts and kidneys (only for long-term experiments) for histological evaluation at the end of the observation period.

### Histology

*In vitro* cultured islets were fixed in 10% formalin and embedded in 4% agar for histological examination using immunofluorescent double-staining of insulin and Hypoxyprobe. Guinea pig anti-insulin (1:400; Agilent Technologies, Santa Clara, CA, USA) and Hypoxyprobe Kit (Hypoxyprobe, Burlington, MA, USA) were used as previously described [40,49,50].

Subcutaneously transplanted islet grafts were resected and fixed in modified Davidson's fixative for histological examination [51]. Masson's trichrome and immunohistochemistry (IHC) staining were performed. Rabbit anti-von Willebrand factor (vWF; 1:200; Agilent Technologies) and guinea pig anti-insulin (1:1500) were used as primary IHC antibodies. Images were captured using an IX50 fluorescence microscope (Olympus, Tokyo, Japan). Positive areas on vWF slides were highlighted in red using cellSens software for visualization (Olympus). Kidneys were fixed in 10% formalin for sectioning. Periodic acid-Schiff (PAS) staining was performed for evaluation of the glomerulus. Glomerulus area and PAS-positive area were quantitated using cellSens software (Olympus), to calculate the % PAS-positive area per glomerulus.

### Statistics

Data are reported as mean ± standard error of the mean. Statistical analysis was performed using JMP 13 (SAS Institute, Cary, NC, USA). $P < 0.05$ was considered statistically significant.

## Results

### Sandwiching islets using mesh maintains islet viability and alleviates aggregation-induced hypoxia *in vitro*

To modify islet graft shape and limit aggregation *in vitro*, we developed a method using Vicryl mesh. We manually modified the original Vicryl mesh, which is finely woven, to a coarser weave of 200-μm mesh size (Fig. 1a). To sandwich isolated rat islets between two mesh layers, we suspended them in fibrin-thrombin gel for temporary fixation [22,40]. As a control, we loaded the same number of islets dispersed in the same amount of gel (Fig. 1b), but without mesh. All islets were cultured *in vitro* for 7 days. During this time, we observed islet aggregation and degradation in the control group. In contrast, the sandwiched islets were well-maintained, without aggregation, within the mesh layers. To evaluate the maintenance of islet volume, we used islets isolated from LUC transgenic rats (Fig. 1c), which maintained significantly greater volume in the mesh group compared to the control group (Fig. 1d, $P = 0.0027$). Next, we assessed the effects of aggregation on the viability and function of cultured islets. We performed viability assays using FDA and PI staining (Fig. 1e). We measured the size of islets (and islet aggregates) in both groups, which demonstrated a significant difference in area [510 290 ± 121 161 $\mu m^2$ (CTL) vs. 13 198 ± 1986 $\mu m^2$ (mesh), $P < 0.0001$, Fig. 1f]. For reference, these average islet areas correspond to islet diameters of 806 μm (CTL) and 130 μm (mesh), on the assumption that islet shape is spherical. Quantitative analysis of viability relative to islet size confirmed significantly higher viability in the mesh compared to control group (Fig. 1g, 55.0 ± 7.1% [CTL] vs. 89.2 ± 1.4% [mesh], $P = 0.0091$). We used GSIS to examine islet function on day 7, normalized using total insulin content in islets (Fig. 1h). Islets in both groups responded to glucose stimulation, and stimulation indices were not

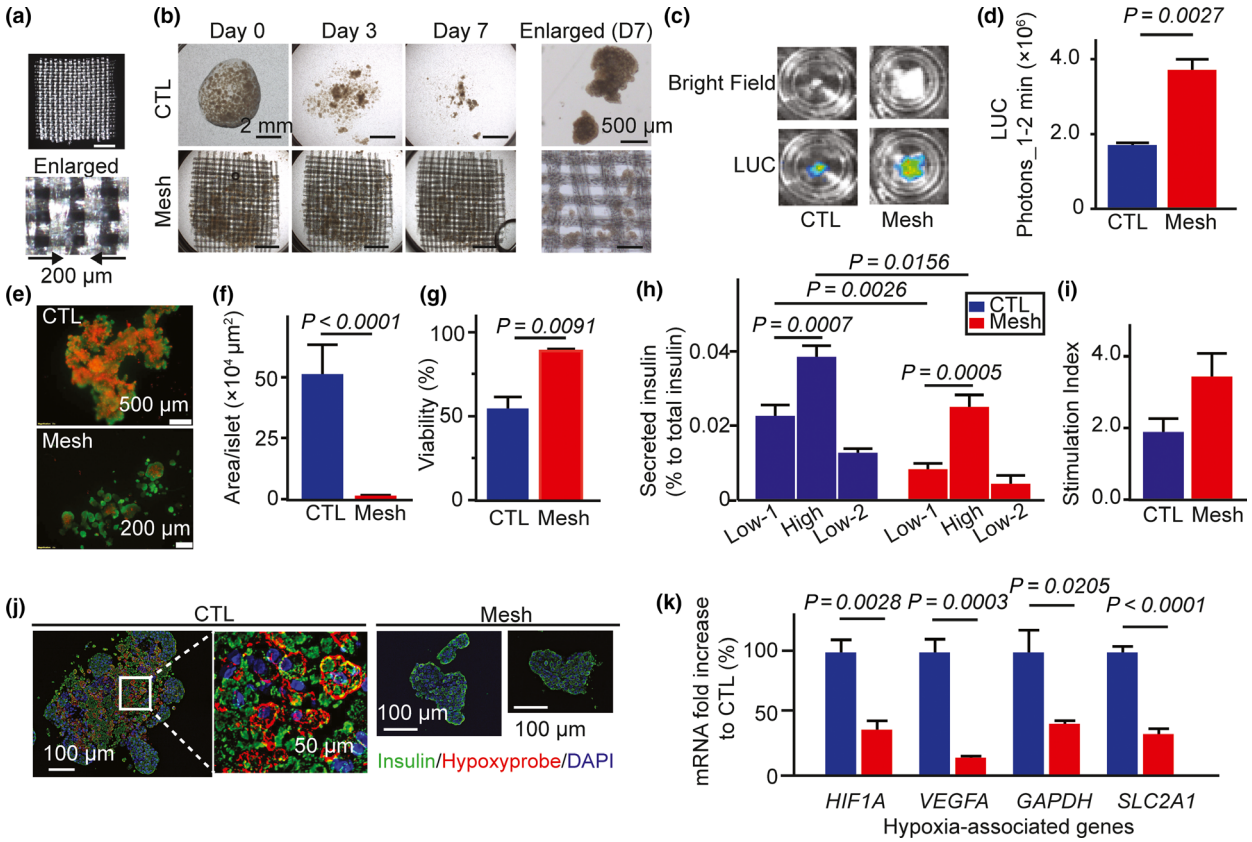


**Figure 1** Using mesh to modify graft shape alleviates aggregation-induced hypoxia and maintains viability *in vitro*. (a) Vicryl mesh was modified to 200-μm mesh size. Upper panel: overview; scale bar: 1 mm. Bottom panel: enlarged. (b) Representative time course of islet appearance in culture for 7 days ($n$ = 4). Three hundred islets were mixed with thrombin–fibrin gel with mesh (two 5 × 5-mm Vicryl mesh layers) or without mesh (control, CTL). A photograph of CTL on Day 0 was taken before applying culture medium, to demonstrate the outline of the gel. Other photographs were taken in culture medium. Scale bar: 2 mm; 500 μm in enlarged photographs. (c) Representative photographs of *in vitro* islet functional volume assessment. Images were captured using ATP-based bioluminescence imaging after a 7-day culture of islets isolated from LUC transgenic rats. (d) Quantitation of LUC bioluminescence showed a significant volume decrease in CTL compared to the mesh group. $n$ = 3. (e) Representative viability assay using FDA (green for live cells) and PI (red for dead cells) in CTL islets and islets retrieved from mesh scaffold. Scale bar: 500 μm in CTL, 200 μm in mesh. (f) Area assessment of islets and islet aggregates demonstrated a significantly larger islet area in CTL due to aggregation compared to the mesh group. $n$ = 8 in CTL and $n$ = 61 in mesh group, total islets and islet aggregates obtained from three individual experiments. (g) Area-based assessment demonstrated improved viability in the mesh group compared to CTL. $n$ = 3. (h) GSIS normalized using total islet insulin content, in three phases of low–high–low-glucose conditions. $n$ = 5. (i) Stimulation indices did not differ significantly between CTL and mesh groups. $n$ = 5. (j) Histology of 7-day cultured CTL islets and islets retrieved from mesh. Immunofluorescent stain for insulin (green), Hypoxyprobe (red), and DAPI (blue) showed hypoxia was more pronounced in CTL islets (left) than in islets retrieved from mesh (right). (k) Gene expression of indicated hypoxia-related genes was significantly suppressed in the mesh group compared to CTL. $n$ = 4.

significantly different (Fig. 1i). We further investigated the $O_2$ microenvironment within islet structures. Aggregated clusters in the control group demonstrated remarkable core hypoxia, detected using Hypoxyprobe (for detection of physical hypoxia in cells exposed to <10 mmHg $pO_2$ [49,50]; Fig. 1j). In contrast, islets retrieved from the layered mesh were well-maintained, without hypoxic cores. To further demonstrate the presence of physiological hypoxia, we analyzed islets for expression of hypoxia-related genes (*HIF1A*, *VEGFA*, *GAPDH*, and *SLC2A1*; Fig. 1k) [13,52-55]. Hypoxia-related gene expression was significantly downregulated in the mesh group compared to the nonmesh control group. Note that although it is commonly used as a housekeeping gene, *GAPDH* is affected by the $O_2$ environment; for this reason, we used *ACTB* for normalization, which is independent of the $O_2$ environment. Collectively, our data show that modification of graft shape using mesh alleviates aggregation-induced hypoxia in islet culture.



Transplant International 2020; 33: 806–818

### $O_2$ simulation reveals that aggregation induces post-transplant lethal hypoxia in the SC site, which is reduced in mesh-sandwiched grafts

To illustrate $O_2$ distribution in subcutaneously transplanted islets, we performed a computational simulation of $O_2$ distribution inside a large aggregate (Fig. S2a, 700 μm diameter, the representative aggregate size in Fig. S1d) in the SC site. The simulation revealed a steep $O_2$ decrease toward the islet core, with 41% of the graft volume exposed to lethal hypoxia (<0.1 mmHg partial pressure of $O_2$ [$pO_2$]) [56]. To demonstrate proof of concept that hypoxia can be mitigated by graft shape modification, we performed a computational simulation of 150-μm diameter islets (average human islet size [57]) uniformly distributed between mesh layers (Fig. S1b). This simulation revealed that the graft volume exposed to lethal hypoxia was reduced to 7.3%.

### Graft shape modification with mesh enhances engraftment in SC islet transplantation

Islets transplanted into the SC site form aggregates, causing lethal hypoxia in the core. Because hypoxia is known to induce post-transplant islet death, we applied our graft modification approach to a model of SC syngeneic islet transplantation in STZ-induced diabetic rats (Fig. 2a, timeline). Transplant procedures for mesh-sandwiched islets are shown in Fig. 2b; because preparation of a prevascularized graft bed is proven to enhance the engraftment of SC-transplanted islets [14-17], in this study, we transplanted 600 islets from LUC donors into a prevascularized SC pocket in both mesh and control groups. We measured changes in post-transplant blood glucose and body weight for 6 weeks; we observed a greater decrease in blood glucose (Fig. 2c and Fig. S3a) and greater weight gain (Fig. 2d and Fig. S3b) in the mesh group compared to the control group, indicating an alleviation of islet glucotoxicity in the mesh group. To assess the *in vivo* viability of transplanted islets, we quantitated LUC intensity (Fig. 2e,f); the mesh group demonstrated significantly higher LUC intensity compared to the control group at both 1 and 3 weeks. To assess islet graft function, in week 5 we examined glucose-stimulated C-peptide secretion and IPGTT. Serum C-peptide levels were significantly increased following glucose stimulation in the mesh group but not in the control group (Fig. 2g); the stimulation index also increased but did not show statistical significance (Fig. 2h). IPGTT demonstrated improved glucose tolerance in the mesh group compared to the control group (Fig. 2i,j). Histological examination of resected graft tissue revealed large aggregations in the control group; in contrast, grafts were maintained as thin layers in the mesh group (overview in Fig. 2k,l; photographs at high magnification in Fig. 2m,n). Although Vicryl mesh is biodegradable, it still remained in the tissue 5 weeks after transplantation. Graft revascularization is critical for maintaining long-term graft viability; to confirm the ability of microvessels to penetrate through the ~200-μm-thick mesh layer, we visualized vessels in the surrounding tissue of the graft. We observed many microvessels penetrating through the mesh structure (detectable as pooled red blood cells visualized with Masson's trichrome [Fig. 2o,p] and as endothelial cells visualized with anti-vWF [Fig. 2q,r]). In addition, we observed limited neutrophil infiltration and minimal fibrotic reactions (visualized with Masson's trichrome) around the graft in the mesh group, comparable to the control group (Fig. 2o,p), indicating minimal inflammatory changes in response to the mesh.

### Long-term graft function is maintained during biodegradation of the mesh

The use of a biodegradable scaffold avoids long-lasting foreign body reactions; however, the effect of mesh degradation on islet grafts is not well understood. Furthermore, because revascularization was well-established by 5 weeks (Fig. 2), a scaffold may not be necessary for the prevention of aggregation-induced hypoxia once graft revascularization is established. Therefore, to further investigate the clinical applicability of using a biodegradable scaffold in the SC site, we examined long-term graft function until the completion of mesh absorption at three months. Because 600 islets with mesh decreased blood glucose by ~200 mg/dl on average but did not achieve euglycemia in short-term experiments (Fig. 2c), for this longer-term experiment, we used 750 islets and assessed whether more islets contributed to improved glycemic control. In the mesh treatment group but not the control group, we observed a steady decrease in blood glucose level during the first 4 weeks, followed by a plateau that did not return to pretransplantation glucose levels (Fig. 3a), indicating that graft function was maintained until the end of the 12-week observation. However, increased islet dose (750 islets) did not contribute to significantly decreased blood glucose by 12 weeks compared to that of 600 islets at 6 weeks (Fig. 2c). Importantly, histological examination at 12 weeks revealed that the Vicryl mesh layers were completely absorbed, while grafts were

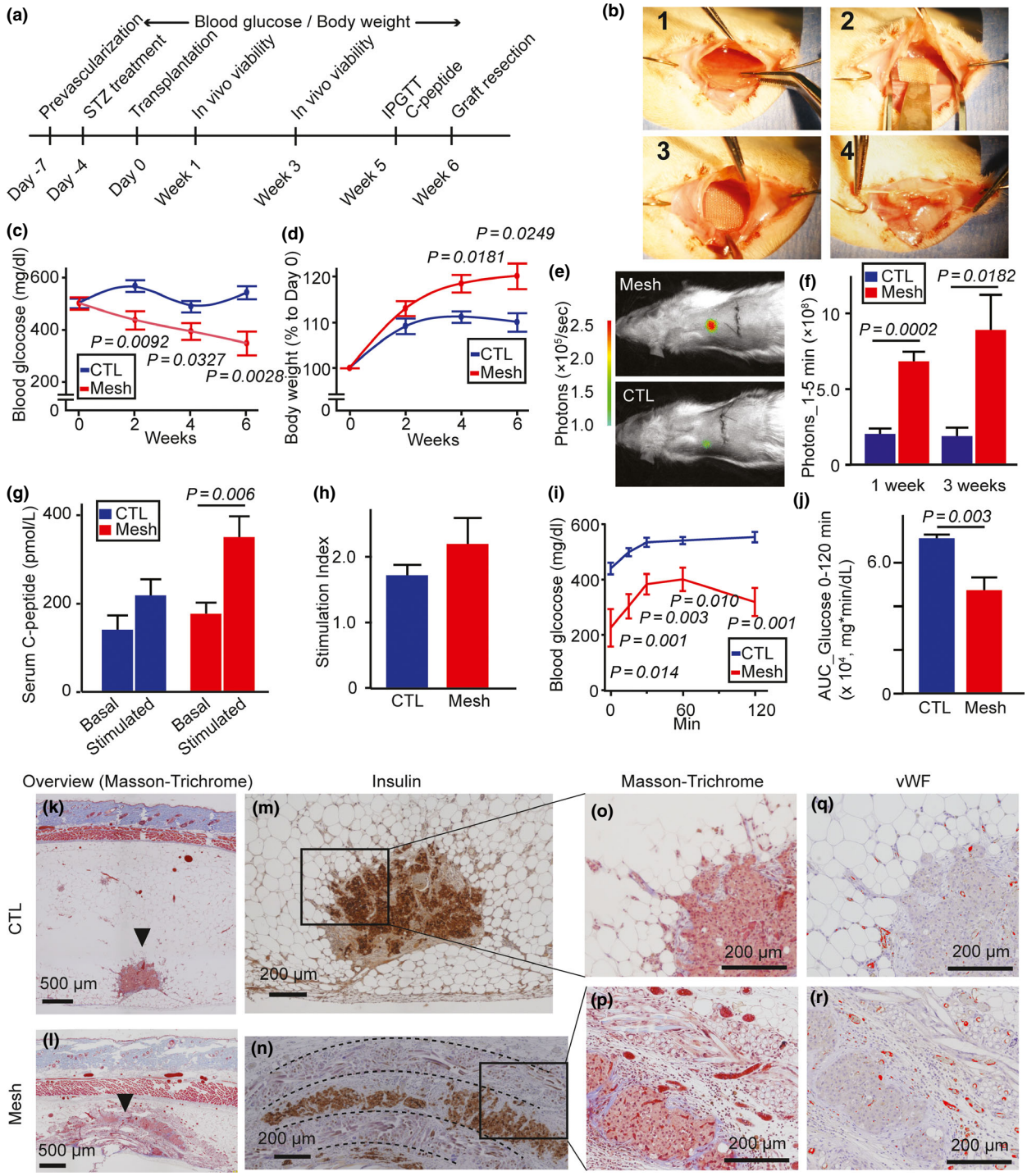


maintained as flat, small clusters (Fig. 3b–e). Furthermore, we observed few inflammatory cells and minimal fibrotic reaction around the graft, and high endothelial cell density around the graft was maintained. Taken together, our functional assessments and histological examinations indicate that Vicryl mesh does not induce unfavorable effects on graft survival during the long-term period of absorption.

After we demonstrated long-term maintenance of graft function for 12 weeks, we further investigated the long-term effect of an SC islet graft on diabetic nephropathy, the major complication associated with diabetes [58,59], which impacts a patient's quality of life. We performed histological examinations (PAS staining) to examine ECM accumulation in the glomerulus as an indicator of nephropathy (Fig. 3f–h)



Transplant International 2020; 33: 806–818

**Figure 2** Graft shape modification with mesh enhances engraftment in SC islet transplantation. (a) Timeline of experiment. (b) Transplant procedures for mesh-sandwiched 600-islet grafts: (1) opening the prevascularized pocket to remove the lyophilized gel disk containing bFGF; (2) insertion of the graft sandwiched between mesh layers; (3) placement of the graft in the SC pocket; and (4) closure of the pocket. (c) Post-transplant blood glucose change demonstrated a larger drop in the mesh group than CTL in a 6-week observation. $n = 7$ for CTL and $n = 8$ for mesh groups. (d) Post-transplant body weight gain improved in the mesh group compared to CTL. $n = 7$ for CTL and $n = 8$ for mesh groups. (e) Representative figure of *in vivo* viability assay performed on day 7, using LUC transgenic rats as donors. $n = 5$ per group. (f) Analysis of bioluminescent intensity illustrated higher viability in the mesh group than in CTL at both weeks 1 and 3. (g) Glucose-stimulated (2 g glucose/kg body weight) C-peptide secretion showed significantly improved responses in the mesh group compared to CTL in absolute C-peptide measurement. $n = 7$ for CTL and $n = 8$ for mesh groups. (h) Stimulation index (C-peptide_60 min/C-peptide_0 min) analysis calculated using C-peptide measurements did not show a significant difference between the groups. (i) IPGTT (2 g glucose/kg body weight) at week 5 demonstrated improved glucose tolerance in the mesh group compared to CTL, demonstrating significantly lower blood glucose at all time points. $n = 7$ for CTL and $n = 8$ for mesh groups. (j) Area under the curve (AUC) analysis of IPGTT demonstrated better glucose tolerance in the mesh group than in CTL. (k–r) Histological examinations of resected grafts. Overview of the grafts using Masson's trichrome staining revealed that CTL grafts demonstrated large aggregates (k), whereas mesh layers held the graft as a thin layer (l). Arrowhead: graft, scale bar: 500 μm. Detailed appearance of the graft using insulin IHC in CTL (m) and mesh group (n). Dotted lines indicate margins of Vicryl layers. Enlarged micrographs of Masson's trichrome (o and p) illustrated that fibrotic changes in the mesh group were minimal and comparable to those in CTL. IHC stain for vWF (q and r) was analyzed, and vWF-positive area was visualized as red by the imaging software (cellSens; Olympus). High vessel density in the surrounding tissue adjacent to the mesh structure was demonstrated in the mesh group. Scale bar: 200 μm in (M-R).

[59-61]. Quantitative analysis revealed that ECM accumulation was significantly greater in the control group compared to the pretransplant and mesh groups (Fig. 3i). Comparing the mesh and pretransplant groups, the increase in ECM accumulation was not significant. Collectively, our results suggest that

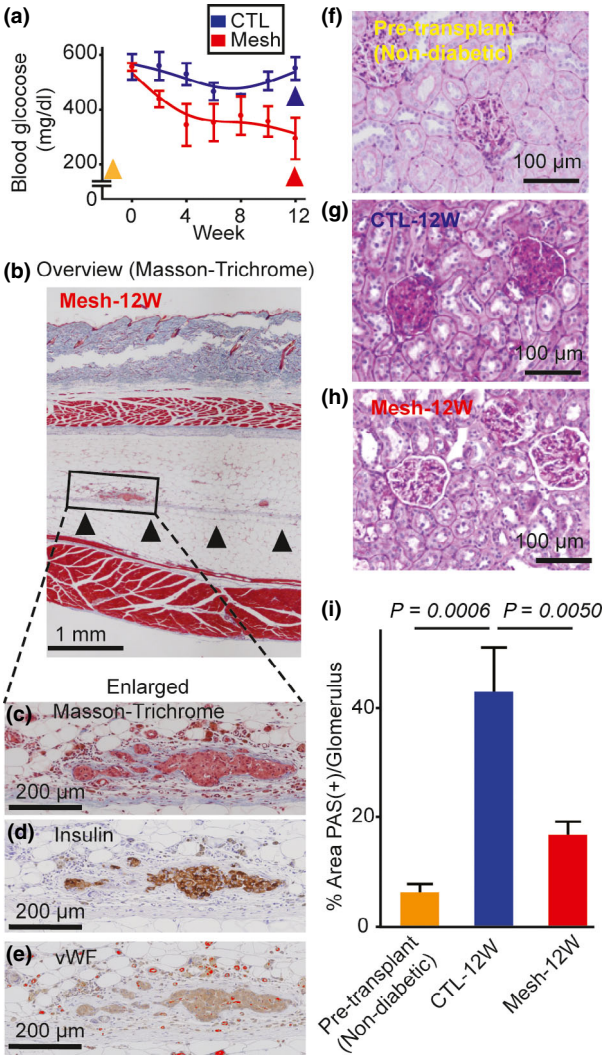


**Figure 3** Long-term (12 weeks) graft function is maintained during the mesh biodegradation period. Long-term graft function (12 weeks) was examined in rats transplanted with 750 islets with or without Vicryl mesh. $n = 4$ for CTL and mesh groups for all experiments. (a) Long-term post-transplant blood glucose change demonstrated a constant decrease in the first 4 weeks and then reached a plateau. (b–e) Representative histology sections at 12 weeks. (b) Overview of Masson's trichrome stain showed that the Vicryl mesh was completely absorbed, with only a trace of the layer detectable as a thin fibrous tissue (arrowheads). (c) Enlarged micrographs of Masson's trichrome stain revealed minimal fibrosis. (d) Insulin stain demonstrated a well-maintained, flat islet graft. (e) vWF showed well-vascularized surrounding tissue as well as islet graft; the image was analyzed, and vWF-positive area was visualized as red (cellSens, Olympus). (f–i) The long-term effect (12 weeks) of mesh-supported islet transplantation on diabetic nephropathy was investigated. Representative PAS staining of kidney sections in pretransplant (f), in CTL group at 12 weeks (g), and in mesh group at 12 weeks (h). Glomeruli in CTL group at 12 weeks demonstrated severe mucopolysaccharides deposition. Scale bar: 100 μm. (i) ECM accumulation was quantified as % PAS-positive area/glomerulus area, demonstrating significantly reduced mucopolysaccharide deposition in the mesh group compared to CTL. Histological quantification was performed by cellSens software (Olympus). More than eight glomeruli were analyzed to calculate the average in a rat.

mesh-dispersed SC islet transplantation effectively alleviates the progression of diabetic nephropathy.

## Discussion

In this report, we introduced a clinically applicable approach to improve SC islet transplantation using biodegradable Vicryl mesh. Transplantation of sandwiched islets between Vicryl mesh layers demonstrated improved engraftment in the SC site when compared to transplantation without mesh. We also demonstrated several advantages of the biodegradable scaffold: Islet grafts were well-vascularized through the mesh layers by 6 weeks, and the function of the vascularized grafts was maintained for a 12-week observation, even after mesh degradation. Vicryl mesh supports the engraftment of islets during the early stage of SC islet transplantation and degrades after completion of engraftment in the late stage, avoiding unnecessary foreign body reaction; this would be an ideal characteristic of scaffolding used for clinical SC islet transplantations.

Many types of scaffolds have been explored to support improved cell transplantation, especially for extrahepatic islet transplantations. For example, a macroporous, biodegradable, poly(lactide-co-glycolide) scaffold with 250–425 μm pore size was used to support islets in the epididymal fat pad of STZ-induced diabetic mice to reverse diabetes [20]. An absorbable scaffold, the Ethisorb Dura Patch (Codman, Raynham, MA, USA), was utilized in a dog autotransplantation model; isolated islets were loaded on the scaffold and wrapped by the omentum, with some transplants achieving insulin independence [21]. However, except for one example of islets loaded on a macroporous, polydimethylsiloxane-based scaffold displaying hypoxia resistance *in vitro* [22], the role of scaffolds on the $O_2$ microenvironment in grafts has not been thoroughly investigated. Because pancreatic islets are highly hypoxia-susceptible, and exogenous oxygenation improves engraftment [13,19,62-64], prevention of hypoxia is an important strategy. Therefore, clarifying the effect of scaffolds on the $O_2$ microenvironment is critically important for designing scaffolds that improve islet transplantation efficiency. In the present study, we demonstrated that scaffolds support improved $O_2$ distribution in islet grafts, by modulating the graft shape to minimize the $O_2$ gradient. We prepared a 200-μm mesh to sandwich isolated islets as a thin layer between the meshes. Because the size of isolated islets widely varies, typically ranging between 50 and 500 μm, some islets may fall into the mesh pores. Although we successfully used thrombin–fibrin gel to hold islets and prevent loss of small islets prior to islet transplantation, mesh size may require additional optimization.

In this study, we combined two approaches to overcome the critical shortcomings in SC islet transplantation: prevascularization of the SC graft bed and graft shape modification by a scaffold. The endogenous tissue $O_2$ level of SC tissue is 45 mmHg, similar to that of the conventional islet transplantation site, the liver (46–50 mmHg) [13,65]. Intriguingly, increasing the vascular density of the graft bed does not increase the $O_2$ level of the SC interstitial space [13]; however, it enhances graft oxygenation via improved replenishment of $O_2$ supply. Prevascularization may also be important for facilitating rapid revascularization of the graft, especially in the case of a nonencapsulated graft that allows direct revascularization, as in our animal model in this study. Because the mechanisms by which prevascularization and scaffold-supported graft shape modification enhance oxygenation are different, a combination of these approaches may show synergy in clinical settings. Additionally, to limit the risk of surgical site infection and ultimately reduce patients' burdens, a one-step SC-site islet transplantation without prevascularization would be an ideal strategy that should be addressed in subsequent studies.

In addition to improving short-term islet transplantation outcomes by preventing aggregation-induced hypoxia, our study also considered the potentially adverse effects of a foreign body reaction to the mesh material during long-term graft maintenance. Vicryl mesh is fully biodegraded into lactic acid and glycolic acid by hydrolysis and absorbed within 8–10 weeks [66]. We showed that islet graft revascularization was established by the time mesh absorption was complete, which in theory requires no scaffolded support for islets thereafter. This explains the maintenance of graft function during our long-term observation (stable blood glucose and reduced kidney damage), with minimal graft inflammation and fibrosis. Because completion of revascularization is reported to take 10 days–1 month [31-35], which is shorter than the absorption period for Vicryl mesh, use of mesh that biodegrades faster may further minimize tissue reactions to enhance engraftment [67]. This could be modified by adding L-lactide (a material commercially available as Vicryl rapide™; Ethicon), and such options could be considered for optimizing clinical application of this approach.

The SC site provides extensive space for clinical islet transplantations, which require an ample transplantation area that allows for minimally invasive procedures



Transplant International 2020; 33: 806–818

and postoperative care. Clinical application of islet transplantation to treat T1D typically requires >300 000 islet equivalents [10,57,68]; to achieve the islet seeding density used in this study, a 12 × 12-cm SC site would be needed to seed enough islets to support clinical transplantation. However, this estimate may vary, as clinical transplantation is allogeneic and a prevascularization method has not yet been established. In addition, seeding density within the SC graft site may affect outcome and should be determined carefully, because a higher seeding density may exacerbate the low $O_2$ environment. Indeed, use of 750 islets did not demonstrate improved glycemic control compared to use of 600 islets in the same sized mesh, which may be attributed to its attendant higher seeding density.

At present, the engraftment efficiency of SC-site islet transplantation using prevascularization and Vicryl mesh scaffolding still needs improvement as an alternative approach to the current clinical practice of intrahepatic islet transplantation. Our group previously demonstrated that intrahepatic transplantation of 600 syngeneic islets reversed diabetes in 83% of LEW rats [38], which is greater than diabetes reversal for SC transplantation with prevascularization and Vicryl mesh introduced in this study; therefore, an additional approach, such as active oxygenation [13,19,62], is required to achieve comparable transplantation efficiency to the conventional intrahepatic site. In fact, with prevascularization of the SC site but without Vicryl mesh support, we showed that 600 islets reversed diabetes in 63% of LEW rats that received active graft oxygenation via post-transplant $O_2$ inhalation [13]. This $O_2$ inhalation strategy may easily be combined with the Vicryl mesh scaffold we introduced in this study, to augment islet engraftment in the SC site.

Our results may be limited by the sex-mismatched transplantation model used in this study. Sex mismatch has been reported as a negative predictor of graft success in allotransplantations in several organs, potentially due to immunologic factors (e.g., production of anti-HLA antibodies) or genetic factors (e.g., development of H-Y antibodies) [69-72], which suggests that sex-matching in SC islet transplantations using Vicryl mesh may further improve outcomes. In addition, a strategy to protect the graft from adaptive immune reactions should be addressed in clinical allotransplantations, although hypoxia-induced graft loss, the focus of the present study, is an independent problem from adaptive immune reactions.

For future SC cell transplantations, our method can be expanded to support stem cell-based treatments, although progenitor and fetal islet cells are less susceptible to hypoxia compared to the nonproliferating mature adult islets [73,74]. Encapsulation is considered a prerequisite for immunoisolation, as well as for retrievability due to the inherent tumorigenic potential of stem cell-derived cells [75]; however, recent advancements in immunoprotection strategies and prevention of tumorigenesis suggest that stem cell-derived cell transplantation has the potential to become a reality, even without encapsulation [76-78]. Although our setup was designed as an open scaffolding for adult islet transplantations, use of clinically established Vicryl mesh as a scaffold will be a powerful tool for SC transplantations using mature or stem cell-derived cells.

## Authorship

HK: designed the study, collected and analyzed data, and wrote the manuscript. NG, MS, CC, JL, and JR: collected data. KO, YT, FK, and YM: reviewed and edited the manuscript.

## Funding

This study was supported by a grant from the Nora Eccles Treadwell Foundation (Title of Grant: CURE OF DIABETES, Grant Period: July 1, 2012–June 30, 2020, P.I.: Yoko Mullen, MD, PhD).

## Conflict of interest

All authors certify that there is no conflict of interest with any financial organization regarding the material discussed in the manuscript.

## Acknowledgements

We thank Mitsuo Kato, Ph.D. and Maryam Abdollahi, Ph.D. for supporting the histology analysis of the kidney sections; Sarah T. Wilkinson, Ph.D. for critical reading and editing of the manuscript; and Taro Yoshida for figure production.

## SUPPORTING INFORMATION

Additional supporting information may be found online in the Supporting Information section at the end of the article.

**Figure S1.** Islets infused into the liver scatter to settle but subcutaneously transplanted islets form large aggregates.

**Figure S2.** $O_2$ simulation reveals that islet aggregation is a major contributor to induction of intra-islet hypoxia, which is alleviated by sandwiching the islet graft.

**Figure S3.** Blood glucose and body weight change data per individual rat.

## REFERENCES


1. Palumbo A, Cavallo F, Gay F, *et al.* Autologous transplantation and main -tenance therapy in multiple myeloma. *N Engl J Med* 2014; **371**: 895.
2. Schmitz N, Pfistner B, Sextro M, *et al.* Aggressive conventional chemotherapy compared with high-dose chemotherapy with autologous haemopoietic stem-cell transplantation for relapsed chemosensitive Hodgkin's disease: a randomised trial. *Lancet* 2002; **359**: 2065.
3. Biernaskie JA, McKenzie IA, Toma JG, Miller FD. Isolation of skin-derived precursors (SKPs) and differentiation and enrichment of their Schwann cell progeny. *Nat Protoc.* 2006; **1**: 2803.
4. Lin H, Liu F, Zhang C, *et al.* Pluripotent hair follicle neural crest stem-cell-derived neurons and schwann cells functionally repair sciatic nerves in rats. *Mol Neurobiol* 2009; **40**: 216.
5. Kroon E, Martinson LA, Kadoya K, *et al.* Pancreatic endoderm derived from human embryonic stem cells generates glucose-responsive insulin-secreting cells in vivo. *Nat Biotechnol.* 2008; **26**: 443.
6. Pagliuca FW, Millman JR, Gurtler M, *et al.* Generation of functional human pancreatic beta cells in vitro. *Cell* 2014; **159**: 428.
7. Rezania A, Bruin JE, Arora P, *et al.* Reversal of diabetes with insulin-producing cells derived in vitro from human pluripotent stem cells. *Nat Biotechnol* 2014; **32**: 1121.
8. Ricordi C. Islet transplantation: a brave new world. *Diabetes* 2003; **52**: 1595.
9. Ryan EA, Lakey JR, Rajotte RV, *et al.* Clinical outcomes and insulin secretion after islet transplantation with the Edmonton protocol. *Diabetes* 2001; **50**: 710.
10. Shapiro AM, Ricordi C, Hering BJ, *et al.* International trial of the Edmonton protocol for islet transplantation. *N Engl J Med* 2006; **355**: 1318.
11. Naziruddin B, Iwahashi S, Kanak MA, Takita M, Itoh T, Levy MF. Evidence for instant blood-mediated inflammatory reaction in clinical autologous islet transplantation. *Am J Transplant.* 2014; **14**: 428.
12. Martin BM, Samy KP, Lowe MC, *et al.* Dual islet transplantation modeling of the instant blood-mediated inflammatory reaction. *Am J Transplant* 2015; **15**: 1241.
13. Komatsu H, Rawson J, Barriga A, *et al.* Posttransplant oxygen inhalation improves the outcome of subcutaneous islet transplantation: a promising clinical alternative to the conventional intrahepatic site. *Am J Transplant* 2018; **18**: 832.
14. Luan NM, Iwata H. Long-term allogeneic islet graft survival in prevascularized subcutaneous sites without immunosuppressive treatment. *Am J Transplant* 2014; **14**: 1533.
15. Pepper AR, Gala-Lopez B, Pawlick R, Merani S, Kin T, Shapiro AM. A prevascularized subcutaneous device-less site for islet and cellular transplantation. *Nat Biotechnol* 2015; **33**: 518.
16. Pileggi A, Molano RD, Ricordi C, *et al.* Reversal of diabetes by pancreatic islet transplantation into a subcutaneous, neovascularized device. *Transplantation* 2006; **81**: 1318.
17. Stiegler P, Matzi V, Pierer E, *et al.* Creation of a prevascularized site for cell transplantation in rats. *Xenotransplantation* 2010; **17**: 379.
18. Chendke GS, Faleo G, Juang C, *et al.* Supporting survival of transplanted stem-cell-derived insulin-producing cells in an encapsulation device augmented with controlled release of amino acids. *Adv Biosyst* 2019; **3**: 1900086.
19. Barkai U, Weir GC, Colton CK, *et al.* Enhanced oxygen supply improves islet viability in a new bioartificial pancreas. *Cell Transplant* 2013; **22**: 1463.
20. Gibly RF, Zhang X, Graham ML, *et al.* Extrahepatic islet transplantation with microporous polymer scaffolds in syngeneic mouse and allogeneic porcine models. *Biomaterials* 2011; **32**: 9677.
21. Kin T, O'Neil JJ, Pawlick R, Korbutt GS, Shapiro AM, Lakey JR. The use of an approved biodegradable polymer scaffold as a solid support system for improvement of islet engraftment. *Artif Organs* 2008; **32**: 990.
22. Pedraza E, Brady AC, Fraker CA, *et al.* Macroporous three-dimensional PDMS scaffolds for extrahepatic islet transplantation. *Cell Transplant* 2013; **22**: 1123.
23. Najjar M, Manzoli V, Abreu M, *et al.* Fibrin gels engineered with pro-angiogenic growth factors promote engraftment of pancreatic islets in extrahepatic sites in mice. *Biotechnol Bioeng* 2015; **112**: 1916.
24. Weaver JD, Headen DM, Aquart J, *et al.* Vasculogenic hydrogel enhances islet survival, engraftment, and function in leading extrahepatic sites. *Sci Adv.* 2017; **3**: e1700184.
25. Stendahl JC, Kaufman DB, Stupp SI. Extracellular matrix in pancreatic islets: relevance to scaffold design and transplantation. *Cell Transplant* 2009; **18**: 1.
26. Davis NE, Beenken-Rothkopf LN, Mirsoian A, *et al.* Enhanced function of pancreatic islets co-encapsulated with ECM proteins and mesenchymal stromal cells in a silk hydrogel. *Biomaterials* 2012; **33**: 6691.
27. Komatsu H, Cook C, Wang CH, *et al.* Oxygen environment and islet size are the primary limiting factors of isolated pancreatic islet survival. *PLoS ONE* 2017; **12**: e0183780.
28. Colton CK. Implantable biohybrid artificial organs. *Cell Transplant* 1995; **4**: 415.
29. Kumagai-Braesch M, Jacobson S, Mori H, *et al.* The TheraCyte device protects against islet allograft rejection in immunized hosts. *Cell Transplant* 2013; **22**: 1137.
30. Tibell A, Rafael E, Wennberg L, *et al.* Survival of macroencapsulated allogeneic parathyroid tissue one year after transplantation in nonimmunosuppressed humans. *Cell Transplant* 2001; **10**: 591.
31. Mattsson G, Jansson L, Carlsson PO. Decreased vascular density in mouse pancreatic islets after transplantation. *Diabetes* 2002; **51**: 1362.
32. Svensson J, Lau J, Sandberg M, Carlsson PO. High vascular density and oxygenation of pancreatic islets transplanted in clusters into striated muscle. *Cell Transplant* 2011; **20**: 783.
33. Lau J, Carlsson PO. Low revascularization of human islets when

experimentally transplanted into the liver. *Transplantation* 2009; **87**: 322.
34. Brissova M, Fowler M, Wiebe P, *et al*. Intraislet endothelial cells contribute to revascularization of transplanted pancreatic islets. *Diabetes* 2004; **53**: 1318.
35. Menger MD, Jaeger S, Walter P, Feifel G, Hammersen F, Messmer K. Angiogenesis and hemodynamics of microvasculature of transplanted islets of Langerhans. *Diabetes* 1989; **38** (Suppl 1): 199.
36. Tobias AM, Low DW. The use of a subfascial vicryl mesh buttress to aid in the closure of massive ventral hernias following damage-control laparotomy. *Plast Reconstr Surg* 2003; **112**: 766.
37. Haynes DF, Kreithen JC. Vicryl mesh in expander/implant breast reconstruction: long-term follow-up in 38 patients. *Plast Reconstr Surg* 2014; **134**: 892.
38. Ito T, Itakura S, Todorov I, *et al*. Mesenchymal stem cell and islet cotransplantation promotes graft revascularization and function. *Transplantation* 2010; **89**: 1438.
39. Hakamata Y, Murakami T, Kobayashi E. "Firefly rats" as an organ/cellular source for long-term in vivo bioluminescent imaging. *Transplantation* 2006; **81**: 1179.
40. Coronel MM, Geusz R, Stabler CL. Mitigating hypoxic stress on pancreatic islets via in situ oxygen generating biomaterial. *Biomaterials* 2017; **129**: 139.
41. Komatsu H, Omori K, Parimi M, Rawson J, Kandeel F, Mullen Y. Determination of islet viability using a zinc-specific fluorescent dye and a semi-automated assessment method. *Cell Transplant* 2016; **25**: 1777.
42. Slepchenko KG, Corbin KL, Nunemaker CS. Comparing methods to normalize insulin secretion shows the process may not be needed. *J Endocrinol* 2019; **241**: 149.
43. Komatsu H, Rawson J, Medrano L, *et al*. Optimizing temperature and oxygen supports long-term culture of human islets. *Transplantation* 2019; **103**: 299.
44. Buchwald P. FEM-based oxygen consumption and cell viability models for avascular pancreatic islets. *Theor Biol Med Model* 2009; **6**: 5.
45. Suszynski TM, Avgoustiniatos ES, Papas KK. Oxygenation of the intraportally transplanted pancreatic islet. *J Diabetes Res* 2016; **2016**: 7625947.
46. Avgoustiniatos ES, Colton CK. Effect of external oxygen mass transfer resistances on viability of immunoisolated tissue. *Ann N Y Acad Sci* 1997; **831**: 145.
47. Gonzalez N, Salgado M, Medrano L, Mullen Y, Komatsu H. Isolated pancreatic islet yield and quality is inversely related to organ donor age in rats. *Exp Gerontol* 2019; **128**: 110739.
48. Komatsu H, Cook CA, Gonzalez N, *et al*. Oxygen transporter for the hypoxic transplantation site. *Biofabrication* 2018; **11**: 015011.
49. Olsson R, Olerud J, Pettersson U, Carlsson PO. Increased numbers of low-oxygenated pancreatic islets after intraportal islet transplantation. *Diabetes* 2011; **60**: 2350.
50. Espes D, Lau J, Quach M, Ullsten S, Christoffersson G, Carlsson PO. Rapid restoration of vascularity and oxygenation in mouse and human islets transplanted to omentum may conztribute to their superior function compared to intraportally transplanted islets. *Am J Transplant* 2016; **16**: 3246.
51. Latendresse JR, Warbrittion AR, Jonassen H, Creasy DM. Fixation of testes and eyes using a modified Davidson's fluid: comparison with Bouin's fluid and conventional Davidson's fluid. *Toxicol Pathol* 2002; **30**: 524.
52. Asikainen TM, Schneider BK, Waleh NS, *et al*. Activation of hypoxia-inducible factors in hyperoxia through prolyl 4-hydroxylase blockade in cells and explants of primate lung. *Proc Natl Acad Sci USA* 2005; **102**: 10212.
53. Miao G, Ostrowski RP, Mace J, *et al*. Dynamic production of hypoxia-inducible factor-1alpha in early transplanted islets. *Am J Transplant* 2006; **6**: 2636.
54. Ahn GO, Seita J, Hong BJ, *et al*. Transcriptional activation of hypoxia-inducible factor-1 (HIF-1) in myeloid cells promotes angiogenesis through VEGF and S100A8. *Proc Natl Acad Sci USA* 2014; **111**: 2698.
55. Kubis HP, Hanke N, Scheibe RJ, Gros G. Accumulation and nuclear import of HIF1 alpha during high and low oxygen concentration in skeletal muscle cells in primary culture. *Biochim Biophys Acta* 2005; **1745**: 187.
56. Cao R, Avgoustiniatos E, Papas K, de Vos P, Lakey JRT. Mathematical predictions of oxygen availability in micro- and macro-encapsulated human and porcine pancreatic islets. *J Biomed Mater Res B Appl Biomater* 2020; **108**: 343.
57. Ricordi C. Quantitative and qualitative standards for islet isolation assessment in humans and large mammals. *Pancreas* 1991; **6**: 242.
58. Kanwar YS, Sun L, Xie P, Liu FY, Chen S. A glimpse of various pathogenetic mechanisms of diabetic nephropathy. *Annu Rev Pathol* 2011; **6**: 395.
59. Kato M, Natarajan R. Diabetic nephropathy–emerging epigenetic mechanisms. *Nat Rev Nephrol* 2014; **10**: 517.
60. Wolf G, Ziyadeh FN. Molecular mechanisms of diabetic renal hypertrophy. *Kidney Int* 1999; **56**: 393.
61. Qian Y, Feldman E, Pennathur S, Kretzler M, Brosius FC 3rd. From fibrosis to sclerosis: mechanisms of glomerulosclerosis in diabetic nephropathy. *Diabetes* 2008; **57**: 1439.
62. Ludwig B, Rotem A, Schmid J, *et al*. Improvement of islet function in a bioartificial pancreas by enhanced oxygen supply and growth hormone releasing hormone agonist. *Proc Natl Acad Sci USA* 2012; **109**: 5022.
63. Hughes SJ, Davies SE, Powis SH, Press M. Hyperoxia improves the survival of intraportally transplanted syngeneic pancreatic islets. *Transplantation* 2003; **75**: 1954.
64. Espes D, Lau J, Quach M, Banerjee U, Palmer AF, Carlsson PO. Cotransplantation of polymerized hemoglobin reduces beta-cell hypoxia and improves beta-cell function in intramuscular islet grafts. *Transplantation* 2015; **99**: 2077.
65. Sakai T, Li S, Kuroda Y, Tanioka Y, Fujino Y, Suzuki Y. Oxygenation of the portal vein by intraperitoneal administration of oxygenated perfluorochemical improves the engraftment and function of intraportally transplanted islets. *Pancreas* 2011; **40**: 403.
66. Perisic T, Zhang Z, Foehr P, *et al*. Biodegradable poly (lactic acid-co-glycolic acid) scaffolds as carriers for genetically-modified fibroblasts. *PLoS ONE* 2017; **12**: e0174860.
67. Brackeen AR, Wells MJ, Freed JM. Irradiated polyglactin 910 (Vicryl Rapide) for placement of full-thickness skin grafts. *Dermatol Surg* 2005; **31**: 1707.
68. Ryan EA, Lakey JR, Paty BW, *et al*. Successful islet transplantation: continued insulin reserve provides long-term glycemic control. *Diabetes* 2002; **51**: 2148.
69. Kittleson MM, Shemin R, Patel JK, *et al*. Donor-recipient sex mismatch portends poor 10-year outcomes in a single-center experience. *J Heart Lung Transplant* 2011; **30**: 1018.
70. Tan JC, Wadia PP, Coram M, *et al*. H-Y antibody development associates with acute rejection in female patients with male kidney transplants. *Transplantation* 2008; **86**: 75.

71. Nakasone H, Remberger M, Tian L, *et al*. Risks and benefits of sex-mismatched hematopoietic cell transplantation differ according to conditioning strategy. *Haematologica* 2015; **100**: 1477.
72. Li Z, Mei S, Xiang J, *et al*. Influence of donor-recipient sex mismatch on long-term survival of pancreatic grafts. *Sci Rep* 2016; **6**: 29298.
73. Brown J, Heininger D, Kuret J, Mullen Y. Islet cells grow after transplantation of fetal pancreas and control of diabetes. *Diabetes* 1981; **30**: 9.
74. De Mesmaeker I, Robert T, Suenens KG, *et al*. Increase functional beta-cell mass in subcutaneous alginate capsules with porcine prenatal islet cells but loss with human adult islet cells. *Diabetes* 2018; **67**: 2640.
75. Desai T, Shea LD. Advances in islet encapsulation technologies. *Nat Rev Drug Discov* 2017; **16**: 338.
76. Xu H, Wang B, Ono M, *et al*. Targeted disruption of HLA genes via CRISPR-Cas9 generates iPSCs with enhanced immune compatibility. *Cell Stem Cell* 2019; **24**: 566.e7.
77. Qadir MMF, Alvarez-Cubela S, Belle K, *et al*. A double fail-safe approach to prevent tumorigenesis and select pancreatic beta cells from human embryonic stem cells. *Stem Cell Rep* 2019; **12**: 611.
78. Lee MO, Moon SH, Jeong HC, *et al*. Inhibition of pluripotent stem cell-derived teratoma formation by small molecules. *Proc Natl Acad Sci U S A*. 2013; **110**: E3281.